arXiv:0806.0994v1 [cond-mat.str-el] 5 Jun 2008

Strongly localized quantum crystalline states and behaviour of the dilute jellium model

Salvino Ciccariello
Dipartimento di Fisica "G. Galilei",
Universitá di Padova,
via Marzolo 8, I-35131 Padova, Italy

June 5, 2008

Abstract

We name strongly localized quantum crystalline state (SLQCS) a determinantal wave-function of the single-particle wave-functions obtained by crystalline translations of a wave-function different from zero only within a primitive cell of the considered quantum crystalline phase. SLQCSs accurately reproduce the low density behaviour of the quantum crystals that, as Wigner's crystalline phase of the jellium model, can become very dilute. Our analysis explicitly deals with this system. We show that the SLQCS energy per particle at large dilution (r_s) behaves as $-M_{dl,\sigma}/r_s + C_\sigma/{r_s}^{3/2}$, where $M_{dl,\sigma}$ turns out to be the Madelung constant of the considered cubic symmetry σ and C_σ is a positive constant only numerically determined. Moreover, as the density gets smaller and smaller, each electron becomes more and more confined to the centre of its cell.

PCAS: 05.30.-w, 71.10.Ca, 71.15.Nc, 73.20.Qt

DFPD/08/Th/06

1 Introduction

The *jellium* model [1, 2] is the simplest model of metallic conductors. It approximates the crystalline array of positive ions by a classical, uniform, positive charge density while the valence electrons are described as quantum mechanical particles interacting among themselves and with the electric field of the aforesaid neutralizing charge distribution. In this way, the Hamiltonian of the system, confined at first within a box of volume V, is

$$\begin{aligned} \hat{H} &= \frac{e^2 n^2}{2} \int_V dv \int_V dv' \frac{e^{-\mu|\mathbf{r}-\mathbf{r}'|}}{|\mathbf{r}-\mathbf{r}'|} - e^2 n \sum_{i=1}^{N} \int_V dv \frac{e^{-\mu|\mathbf{r}_i-\mathbf{r}|}}{|\mathbf{r}_i-\mathbf{r}|} \\ &\quad - \sum_{i=1}^{N} \frac{\nabla_i^2}{2m} + \frac{e^2}{2} \sum_{1\le i\ne j\le N} \frac{e^{-\mu|\mathbf{r}_i-\mathbf{r}_j|}}{|\mathbf{r}_i-\mathbf{r}_j|}. \end{aligned} \tag{1}$$

Here, N denotes the number of the electrons contained in the box, $n \equiv N/V$ the electron number density, $\mathbf{r}_i$ the position vector of the ith electron, e and m electrons' charge and mass. The cut-off parameter μ goes to zero after taking the thermodynamic limit: $V \to \infty$, $N \to \infty$ with n fixed. Besides, in Eq. (1) and throughout the paper we adopt units such that $\hbar = 1$.

The first order perturbative approximation of the energy of the fundamental state of $\hat{H}$ was evaluated by Wigner[3] for the unpolarized case and reads

$$E_u = \langle F_u|\hat{H}|F_u\rangle = N\frac{e^2}{2a_0}\left(\frac{2.209}{r_s^2} - \frac{0.916}{r_s}\right) \tag{2}$$

where $|F_u\rangle$ denotes the fundamental state of N free and unpolarized spin 1/2 particles, $a_0 = 1/me^2$ is the Bohr atomic radius, $r_s \equiv r_0/a_0$ the perturbation parameter with $r_0 \equiv (3/4\pi n)^{1/3}$. The corresponding approximation for the polarized case was obtained by Bloch[4] and reads

$$E_p = \langle F_p|\hat{H}|F_p\rangle = N\frac{e^2}{2a_0}\left(\frac{3.508}{r_s^2} - \frac{1.154}{r_s}\right), \tag{3}$$

where $|F_p\rangle$ denotes the fundamental state of N polarized free fermions. Expressions (2) and (3) refer to homogeneous systems. Their comparison shows that the polarized configuration is the one stable at lower density, *i.e.* for $r_s > 5.7$. The energy of the classical crystals, formed by electrons arranged on a lattice with simple (sc) or body (bcc) or face centred cubic (fcc) symmetry and a neutralizing positive uniform background, is $-N(e^2/2a_0)M_{dl,\sigma}/r_s$, where $M_{dl,\sigma}$ with $\sigma = 1, 2, 3$ denotes the Madelung constant respectively equal to 1.76012, 1.79186 or 1.79175[5] for the sc, bcc or fcc case. Since at high dilution these energies become definitely smaller than Eq. (3)'s, Wigner concluded that, at large r_s, the fundamental state of the jellium no longer can be that of the homogeneous Fermi gas at $T = 0^0K$. It must have a crystalline structure. In fact, assuming that each electron oscillates around its equilibrium position and

that these positions form a bcc lattice, Wigner[6] obtained the following energy expression

$$E_{crW} = N\frac{e^2}{2a_0}\left(-\frac{1.79186}{r_s} + \frac{3}{r_s^{3/2}}\right), \tag{4}$$

where the term proportional to r_s^{-1}, representing the energy of the classical crystal, was put in, so to say, by hand. A better approximation was later obtained by Carr[7] expanding, as Wigner did, the electrons' position vectors $\mathbf{r}_j$ around the bcc lattice values and, contrarily to Wigner, also retaining the lowest order terms that couple the resulting harmonic oscillators among themselves. The resulting first order approximation of the fundamental state energy is

$$E_{crC} = N\frac{e^2}{2a_0}\left(-\frac{1.79186}{r_s} + \frac{2.66}{r_s^{3/2}}\right). \tag{5}$$

At large r_s we have $E_{crC} < E_{crW} < E_p$. On the basis of these inequalities one cannot however invoke the Ritz-Rayleigh principle to conclude that at high dilution the jellium model is in a bcc crystalline state because expressions (4) and (5) were not obtained considering the full Hamiltonian $\hat{H}$ of the jellium model, as defined in Eq. (1.1), but two different modifications of it. The property can however be proved showing that the solution, with the bcc symmetry, of the jellium's Hartree-Fock (HF) equation yields an energy lower than Eq. (3)'s at large r_s. To this aim we recall that the solution $\psi(\mathbf{r}_1, \ldots, \mathbf{r}_N)$ of the HF equations is the wave function that has a determinantal structure and minimizes the expectation value of $\hat{H}$[8, 9]. Further, in writing down the determinantal wave-function, one usually assumes that the single particle wave-functions have a particular functional form. In particular, assuming that the single particle wave-functions are the plane waves $e^{i\mathbf{k}_j\cdot\mathbf{r}}$ with $j = 1, \ldots, N$, the resulting HF energy coincides with expressions (2) or (3) depending on the considered polarization degree. On the contrary, a HF crystalline solution can be obtained assuming that the single particle wave-functions $\varphi_j(\mathbf{r})$ have the form $e^{i\mathbf{k}_j\cdot\mathbf{r}}u(\mathbf{r})$, with $j = 1, \ldots, N$ and $u(\mathbf{r})$ a periodic function (with the chosen crystalline symmetry) to be determined through the minimization of the HF energy. Applying this procedure, it was recently found[10] that crystalline HF energies become smaller than Eq. (3)'s at $r_s \geq 4.4$ and that the bcc HF energy is the smallest in the region $r_s > 13.3$. In this way, Wigner's statement that diluted jellium assumes a bcc crystalline configuration is put on a firmer basis because it is now a consequence of the Ritz-Rayleigh principle. Strictly speaking the stability of the crystalline phase cannot be considered rigorously proved because the exact fundamental state is not required to have a determinantal structure, as assumed in the HF equations. However, the statement's validity is also supported by Quantum Monte Carlo (QMC) calculations [11, 12, 13, 14, 15, 16] that, relaxing the determinantal restriction, confirm that the stable phase of the dilute electron jellium is the bcc one (even though the exact r_s value of the transition is not yet well assessed because, depending on the paper, it ranges from 50 to 105).

The aim of this paper is to present a simpler procedure to show the existence, for the jellium model, of crystalline phases more stable than the fluid one and to illustrate how these quantum-mechanical crystalline solutions reproduce the classical crystal behaviours as $r_s \to \infty$. These solutions are essentially obtained by a simplified HF procedure as follows. First, one assumes that the confining box V consists of $N = (2M+1)^3$ primitive cells with the chosen crystalline symmetry. Then, one assumes that the single particle wave-function $\varphi_j(\mathbf{r}, \alpha)$, with $j = 1, \ldots, N$, differs from zero only within the jth primitive cell and goes to zero at the cell's border. Besides, each $\varphi_j(\mathbf{r}, \alpha)$ is obtained translating a normalized function $\phi(\mathbf{r}, \alpha)$ that differs from zero only within $V_{\mathbf{0}}$ (the primitive cell centred at the origin) and goes to zero at the border of $V_{\mathbf{0}}$. The corresponding translation vector is $\sum_{i=1}^{3} m_{j,i}\mathbf{a}_i$, the $\mathbf{a}_i$s being the vectors specifying the primitive cell and $\mathbf{m}_j = (m_{j,1}, m_{j,2}, m_{j,3})$ the vector (with integer components) that labels the jth cell. Finally, α is a parameter to be determined by a variational procedure that will be described later. It must be noted that, if $j \neq k$, functions $\varphi_j(\mathbf{r}, \alpha)$ and $\varphi_k(\mathbf{r}, \alpha)$ are orthogonal because their supports have void intersection. The determinantal wave-function is

$$\psi(\mathbf{r}_1, \ldots, \mathbf{r}_N, \alpha) = \frac{1}{\sqrt{N!}} \sum_P (-1)^P \varphi_1(\mathbf{r}_{i_1}, \alpha)\varphi_2(\mathbf{r}_{i_2}, \alpha) \ldots \varphi_N(\mathbf{r}_{i_N}, \alpha), \qquad (6)$$

where the sum is performed over all the permutations $i_1, i_2, \ldots, i_N$ of $1, 2, \ldots, N$ and $(-1)^P$ is the parity of the considered permutation. Hereafter, wave-function (6) is referred to as a strongly localized quantum crystalline state (SLQCS) if the involved $\varphi_j(\mathbf{r}, \alpha)$s obey the properties mentioned above. Then, one evaluates the expectation value of $\hat{H}$ over the above normalized wave-function. In the thermodynamic and subsequent $\mu \to 0$ limits, the resulting energy expression depends on α and r_s, and one looks for the α value that makes the energy value minimum for each r_s value. In this way one finds (see Fig.1) that: i) the resulting sc, bcc and fcc SLQCS energies become smaller than Eq. (3)'s at $r_s \geq 28$, $r_s \geq 36$ and $r_s \geq 38$, respectively, ii) the SLQCS fcc energy nearly coincides with the bcc one. More definitely, it is always smaller than the bcc's and their slight difference monotonically decreases throughout the explored r_s range $[0, 10^4]$. The sc SLQCS energy at first is smaller that the fcc's and bcc's and becomes greater of the last two at $r_s \geq 500$, iii) the three SLQCS energies approach the relevant Madelung contributions as $r_s \to \infty$. Consequently, the bcc SLQC energy approaches the corresponding leading term of Eq.s (4) and (5), iv) the optimized α value increases with r_s and at large r_s one has $\alpha \propto \sqrt{r_s}$, v)in the same r_s region, the subleading asymptotic terms of the sc, bcc and fcc SLQCS energies are proportional to $r_s^{-3/2}$, and vi) our SLQCS energies are always greater than those obtained in Ref.[10] that lie close to the full circles shown in Fig.1a.

Result vi) is not unexpected because the above HF procedure minimizes $\langle\psi|\hat{H}|\psi\rangle$ over a class of functions that, for the assumption that the $\varphi_j(\mathbf{r}, \alpha)$s have compact support, is more restricted than that used in Ref.[10]. The SLQCS procedure is however interesting for its numerical simplicity and for the choice of

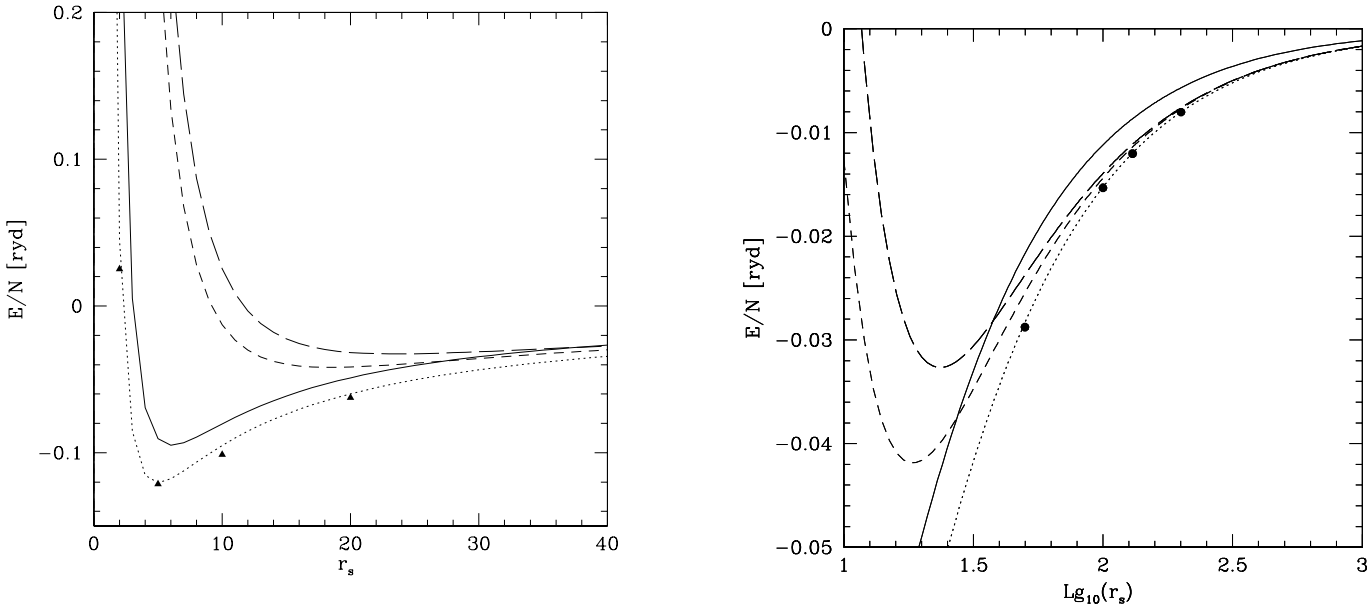

Figure 1: Left and right parts: respectively the energy per particle of the fully polarized jellium model (in Rydberg units) in the inner and outer part of the r_s-range. (Note the r_s logarithmic-scale on the right.) In both figures, the continuous lines refer to Eq. (3), the dotted lines to Carr's bcc expression (5), and the short-dash and the long-dash curves to the SLQC solutions with the sc or the bcc symmetry, respectively. The full triangles and circles correspond to the QMC results of Ref.s [15, 16]. The SLQCS fcc solution is not shown because it lies very close to the bcc.

the single particle wave-functions. The latter's noticed orthogonality property has an important consequence: if we evaluate the expectation value of $\hat{H}$ over the normalized Hartree wave-function

$$\psi_H(\mathbf{r}_1, \ldots, \mathbf{r}_N, \alpha) = \varphi_1(\mathbf{r}_1, \alpha)\varphi_2(\mathbf{r}_2, \alpha) \ldots \varphi_N(\mathbf{r}_N, \alpha), \tag{7}$$

we obtain the same expectation value resulting from the fully antisymmetric state (6). In other words, SLQCSs have the property that the Hartree and the Hartree-Fock equations coincide because the exchange contributions turn out to be equal to zero as it will be explicitly shown below Eq. (23). The equivalence of Eq. (6) with (7) in their final results and the condition that the $\varphi_j(\mathbf{r}, \alpha)$s vanish on their cell borders imply that in the the SLQCS approach each electron in practice is bound to lie within a single cell of the lattice. This feature on the one hand explains why wave-function (6) was named strongly localizedquantum crystalline state. On the other hand, the same feature is shown by classical ionic crystal. Hence, it is not surprising that the quantum-mechanical description, based on SLCQSs, reproduces the classical crystal behaviour in the limit $r_s \to \infty$. This appears already evident from results iii) and iv). In particular result iv) implies that, as $r_s \to \infty$, each electron becomes more and more confined to the centre of the primitive cell that the electron occupies, while result iii) quantum mechanically reproduces the $O(1/r_s)$ term, manually introduced into Eq.s (1.4) and (1.5) by Wigner and Carr.
The derivation of these results will now be detailed according to the following plan. In section 2 we work out the analytical expressions of the expectation value $\langle\psi|\hat{H}|\psi\rangle$ in direct and reciprocal space for the three mentioned cubic symmetries. In section 3 we specify the functional form of $\phi(\mathbf{r}, \alpha)$ and report the relevant numerical results already anticipated at i)-vi). Section 4 concludes the paper. Some mathematical details are left to appendices A and B.

2 Analytical expressions

The primitive cell $V_\mathbf{0}$ centred at the origin is defined as

$$V_\mathbf{0} \equiv \{\mathbf{r} \Big| \ \mathbf{r} = \sum_{i=1}^{3} \frac{\xi_i \mathbf{a}_i}{2}, \ 1 < \xi_i < 1, \ i = 1, 2, 3\}, \tag{8}$$

where the involved $\mathbf{a}_i$s are respectively specified in Eq.s (27a), (29) and (34) of Chapt. 2 of Ref. [17] for the sc, bcc and fcc lattices. For these symmetries the primitive cell volumes are

$$v_0 = a^3, \quad a^3/2, \quad a^3/4, \tag{9}$$

a denoting the cubic lattice spacing. The corresponding r_s values are

$$r_s = (3/4\pi)^{1/3} a/a_0, \quad (3/8\pi)^{1/3} a/a_0 \quad \text{and} \quad (3/16\pi)^{1/3} a/a_0. \tag{10}$$

We define now the wave-function relevant to a SLQCS. To this aim, we first introduce a real even function $\phi(\mathbf{r}, \alpha)$ that differs from zero only within $V_\mathbf{0}$

and depends on a positive real parameter α. Whatever α, $\phi(\mathbf{r},\alpha)$ and its first and second partial derivatives are continuous throughout $V_{\mathbf{0}}$ and vanish as $\mathbf{r}$ approaches the border of $V_{\mathbf{0}}$. Besides, $\phi(\mathbf{r},\alpha)$ is normalized, *i.e.*

$$\int_{V_{\mathbf{0}}} \phi^2(\mathbf{r},\alpha)\, dv = 1, \tag{11}$$

and the α dependence is such that

$$\lim_{\alpha\to\infty} \phi^2(\mathbf{r},\alpha) = \delta(\mathbf{r}), \tag{12}$$

$\delta(\mathbf{r})$ denoting the three-dimensional (3D) Dirac function. Assume now that the box of volume V, where the jellium is confined, contains $(2M+1)$ primitive cells along each direction $\mathbf{a}_i$. Then the jellium will contain $N = (2M+1)^3$ electrons, $V_{\mathbf{0}}$ is one of the possible cells and $v_0 = V/N$. We denote the primitive cells either as $V_{\mathbf{m}}$ (with $-M \le m_i \le M$ and $i = 1,2,3$) or, after performing a convenient relabeling $\mathbf{m} \to \jmath(\mathbf{m})$, as $V_\jmath$ with $\jmath = 1,\ldots,N$. The inverse relabeling exists and reads $j \to \mathbf{m}(j)$. We set now

$$\varphi_{\mathbf{m}}(\mathbf{r},\alpha) = \varphi_\jmath(\mathbf{r},\alpha) \equiv \phi(\mathbf{r} - \sum_{l=1}^{3} m_l \mathbf{a}_l, \alpha). \tag{13}$$

Function $\varphi_{\mathbf{m}}(\mathbf{r},\alpha)$ results from the translation of $\phi(\mathbf{r})$ by $\sum_{l=1}^{3} m_l \mathbf{a}_l$. It differs from zero only within primitive cell $V_{\mathbf{m}}$ and is there normalized. Moreover the $\varphi_{\mathbf{m}}(\mathbf{r},\alpha)$s are orthonormal, *i.e.*

$$\int_V \varphi_j(\mathbf{r},\alpha)\varphi_{j'}(\mathbf{r},\alpha) dv = \delta_{j,j'}, \quad j,j' = 1,\ldots,N. \tag{14}$$

A strongly localized quantum crystalline (SLQC) wave-function is defined as the determinantal function defined by Eq.s (6), (13) and (14). We assume that the normalized wave function of the N polarized electrons is a SLQC wave-function that, by the previous definitions, is normalized within V. With such a function, the electron number density $n(\mathbf{r})$ turns out to be periodic and equal to

$$n(\mathbf{r}) = \sum_{\mathbf{m}} \phi^2(\mathbf{r} + \sum_{i=1}^{3} m_i \mathbf{a}_i, \alpha). \tag{15}$$

As already anticipated, our task now is to evaluate the expectation value $E(N,V,\alpha)$ of $\hat{H}$ over a SLQC wave-function and to choose α so as to make $E(N,V,\alpha)$ as small as possible for each r_s value. After putting

$$\epsilon(r_s,\alpha) \equiv E(N,V,\alpha)/N \equiv \langle\psi|\hat{H}|\psi\rangle/N, \tag{16}$$

from Eq.s (1), (6) and (13) one gets

$$\epsilon(r_s,\alpha) = h_{b-b} + h_{e-b} + \langle\hat{T}\rangle + \langle\hat{V}\rangle \tag{17}$$

with

$$h_{b-b} = \frac{e^2 N}{2V^2} \int_V dv \int_V dv' \frac{e^{-\mu|\mathbf{r}-\mathbf{r}'|}}{|\mathbf{r}-\mathbf{r}'|}, \tag{18}$$

$$h_{e-b} = -\frac{e^2}{V} \sum_{j=1}^{N} \int_{V_0} dv \int_V dv' \frac{\phi^2(\mathbf{r},\alpha) e^{-\mu|\mathbf{r}-\mathbf{r}'+\sum_{i=1}^{3} m_i(j)\mathbf{a}_i|}}{|\mathbf{r}-\mathbf{r}'+\sum_{i=1}^{3} m_i(j)\mathbf{a}_i|}, \tag{19}$$

$$\langle \hat{T} \rangle = \frac{1}{2m} \int_{V_0} \nabla\phi(\mathbf{r},\alpha) \cdot \nabla\phi(\mathbf{r},\alpha) dv, \tag{20}$$

and

$$\langle \hat{V} \rangle = \frac{e^2}{2N} \sum_{1 \le \imath \ne \jmath \le N} \Big[J_{\imath,\jmath} - K_{\imath,\jmath} \Big], \tag{21}$$

where[18]

$$J_{\imath,\jmath} \equiv \int_V dv \int_V dv' {\varphi_\imath}^2(\mathbf{r},\alpha) {\varphi_\jmath}^2(\mathbf{r}',\alpha) \frac{e^{-\mu|\mathbf{r}-\mathbf{r}'|}}{|\mathbf{r}-\mathbf{r}'|}, \tag{22}$$

$$K_{\imath,\jmath} \equiv \int_V dv \int_V dv' \varphi_\imath(\mathbf{r},\alpha)\varphi_\imath(\mathbf{r}',\alpha)\varphi_\jmath(\mathbf{r},\alpha)\varphi_\jmath(\mathbf{r}',\alpha) \frac{e^{-\mu|\mathbf{r}-\mathbf{r}'|}}{|\mathbf{r}-\mathbf{r}'|}. \tag{23}$$

Contributions h_{b-b} and h_{e-b} respectively originate from the first and second term on the right hand side (rhs) of Eq. (1). Property (13) has been used to derive Eq.s (19) and (20). Quantities $J_{\imath,\jmath}$ and $K_{\imath,\jmath}$ represent the direct and the exchange contributions, respectively. The exchange contributions originate from the antisymmetry of the wave-function. In our case it turns out that the $K_{\imath,\jmath}$s with $\imath \neq \jmath$, as the sum present in Eq. (21) requires, are equal to zero owing to the fact that $\varphi_\imath(\mathbf{r},\alpha)$ and $\varphi_\jmath(\mathbf{r},\alpha)$ have supports with a void intersection. Thus, despite the fact that the considered wave-function is antisymmetric, SLQCS are characterized by vanishing exchange contributions. In other words, SLQCSs are defined by the property that the associated Hartree and Hartree-Fock equations yield the same final results. In fact, starting from Eq. (1.7), one easily checks that the resulting expectation of $\hat{H}$ again is the sum of analytical expressions (20) and (27).
Using Eq.s (13) and (22), the sum involving the $J_{\imath,\jmath}$s becomes

$$\sum_{1 \le \imath \ne \jmath \le N} J_{\imath,\jmath} = \sum_{\mathbf{m} \ne \mathbf{m}'} \int_{V_0} dv \int_{V_0} dv' \phi^2(\mathbf{r},\alpha)\phi^2(\mathbf{r}',\alpha) \frac{e^{-\mu|\mathbf{r}-\mathbf{r}'+\sum_{l=1}(m_l-m_l{}')\mathbf{a}_l|}}{|\mathbf{r}-\mathbf{r}'+\sum_{l=1}(m_l-m_l{}')\mathbf{a}_l|}.$$

With the change $(m_l - m_l') \to m_l$ and letting N go to infinity one gets

$$\sum_{1 \le \imath \ne \jmath \le N} J_{\imath,\jmath} \to N {\sum_{\mathbf{m}}}' \int_{V_0} dv \int_{V_0} dv' \phi^2(\mathbf{r},\alpha)\phi^2(\mathbf{r}',\alpha) \frac{e^{-\mu|\mathbf{r}-\mathbf{r}'+\sum_{l=1} m_l\mathbf{a}_l|}}{|\mathbf{r}-\mathbf{r}'+\sum_{l=1} m_l\mathbf{a}_l|}, \tag{24}$$

where $\mathbf{m}$ runs over all the points of the $\mathcal{Z}^3$ lattice excluding the origin. The last restriction is signaled by the prime. Recalling that $V = \cup_{j=1}^{N} V_{\mathbf{m}(j)}$, contribution h_{e-b} can be converted into a double sum, *i.e.*

$$h_{e-b} = -\frac{e^2}{V} \sum_{\mathbf{m},\mathbf{m}'} \int_{V_0} dv \int_{V_0} dv' \frac{\phi^2(\mathbf{r},\alpha) e^{-\mu|\mathbf{r}-\mathbf{r}'+\sum_{i=1}^{3}(m_i-m'_i)\mathbf{a}_i|}}{|\mathbf{r}-\mathbf{r}'+\sum_{i=1}^{3}(m_i-m'_i)\mathbf{a}_i|}.$$

In the thermodynamic limit one finds that

$$h_{e-b} = -e^2 n \sum_{\mathbf{m}} \int_{V_0} dv \int_{V_0} dv' \frac{\phi^2(\mathbf{r},\alpha) e^{-\mu|\mathbf{r}-\mathbf{r}'+\sum_{i=1}^{3} m_i\mathbf{a}_i|}}{|\mathbf{r}-\mathbf{r}'+\sum_{i=1}^{3} m_i\mathbf{a}_i|}. \tag{25}$$

In a similar way one shows that

$$h_{b-b} = \frac{e^2 n^2}{2} \sum_{\mathbf{m}} \int_{V_0} dv \int_{V_0} dv' \frac{e^{-\mu|\mathbf{r}-\mathbf{r}'+\sum_{i=1}^{3} m_i\mathbf{a}_i|}}{|\mathbf{r}-\mathbf{r}'+\sum_{i=1}^{3} m_i\mathbf{a}_i|}. \tag{26}$$

Collecting the above results and taking the limit $\mu \to \infty$ one obtains the contribution of the total Coulombic interaction to the quantum energy per particle, namely

$$\begin{aligned} h_{b-b} + h_{e-b} + \langle \hat{V} \rangle = \frac{e^2}{2} \Big[& - \int_{V_0} dv \int_{V_0} dv' \frac{2n\phi^2(\mathbf{r},\alpha) - n^2}{|\mathbf{r}-\mathbf{r}'|} \\ & + {\sum_{\mathbf{m}}}' \int_{V_0} dv \int_{V_0} dv' \frac{\phi^2(\mathbf{r},\alpha)\phi^2(\mathbf{r}',\alpha) - 2n\phi^2(\mathbf{r},\alpha) + n^2}{|\mathbf{r}-\mathbf{r}'+\sum_{i=1}^{3} m_i\mathbf{a}_i|} \Big]. \end{aligned} \tag{27}$$

We make now three remarks. First, if one assumes that $\phi^2(\mathbf{r},\alpha)$ is a Gaussian function, the rhs of Eq. (27) coincides with the expression reported by Ewald in his calculation of the Coulombic energy per particle for a classical crystal (see *e.g.* Ref.s [19, 20]). However, the introduction of the Gaussian function in Ewald's procedure was only a trick to make the convergence faster, while in the SLQCS procedure $\phi^2(\mathbf{r},\alpha)$ is the quantum probability density of finding an electron at position $\mathbf{r}$. Second, the series present in Eq. (27) is convergent. In fact, setting $A(\mathbf{m})\hat{\nu}(\mathbf{m}) \equiv \sum_{l=1} m_l \mathbf{a}_l$ where $\hat{\nu}(\mathbf{m})$ is a unit vector, the expansion of the denominator, present in Eq. (27), at large $A(\mathbf{m})$ values yields

$$\begin{aligned} \frac{1}{|\mathbf{r}-\mathbf{r}'+A(\mathbf{m})\hat{\nu}(\mathbf{m})|} \quad \approx \quad & \frac{1}{A(\mathbf{m})} \Big[1 - \frac{(\mathbf{r}-\mathbf{r}')\cdot\hat{\nu}(\mathbf{m})}{A(\mathbf{m})} + \\ & + \frac{3(\mathbf{r}-\mathbf{r}')\cdot\hat{\nu}(\mathbf{m}) - (\mathbf{r}-\mathbf{r}')^2}{2A^2(\mathbf{m})} + \ldots \Big]. \end{aligned} \tag{28}$$

The volume integrals of the first term on the rhs is equal to zero. The remaining two terms also yield vanishing contributions provided the sum over $\mathbf{m}$ is first performed over all the $\mathbf{m}$s that have different directions and equal modulus and, subsequently, over the different $|\mathbf{m}|$ values. In this way, as $A(\mathbf{m})$ becomes very large, the first of the resulting sums amounts to performing an angular average

over the directions of $\hat{\nu}(\mathbf{m})$. It is easily checked that the $\hat{\nu}$ dependence of the numerators present in Eq. (28) is such that their angular averages vanish for the sc, fcc and bcc cases. One concludes that the terms of series (27) decrease as $A^{-4}(\mathbf{m})$ at large $\mathbf{m}$s, and the series convergence is proved. Third, owing to condition (12), the limit of Eq. (27) as $\alpha \to \infty$ is the electrostatic energy of a lattice of point-like charges plus a uniform neutralizing charge within each cell (the cubic symmetry being specified by V_0 and the $\mathbf{a}_i$s). Hence, the limit value of the rhs of (27) for $\alpha \to \infty$ is equal to $e^2 M_{dl,\sigma}/2a_0 r_s$ where the $M_{dl,\sigma}$s are the Madelung constants defined below Eq. (3). This remark shows that the SLQC approximation yields the classical crystal energy in the infinite dilution limit because later, after illustrating the results shown in Fig.2, it will appear clear that the limit $r_s \to \infty$ implies that $\alpha \to \infty$.
Before concluding the section, we further elaborate the above expressions in terms of new integration variable $\vec{\xi}$ and dimensionless function $\phi_0(\vec{\xi}, \alpha)$. The new quantities are respectively defined by

$$\mathbf{r} = \sum_{l=1}^{3} \xi_l \mathbf{a}_l/2,$$

and

$$\phi_0(\vec{\xi}, \alpha) \equiv (8/v_0)^{-1/2} \phi(\mathbf{r}, \alpha) = (8/v_0)^{-1/2} \phi(\sum_{l=1}^{3} \xi_l \mathbf{a}_l/2, \alpha). \tag{29}$$

Recalling Eq. (8), the tip of vector $\vec{\xi}$ is confined to the cubic cell C_0 of edge 2 centred at the origin of an orthogonal Cartesian frame and defined as

$$C_0 \equiv \{\vec{\xi} | -1 \leq \xi_j \leq 1, \quad j = 1, 2, 3\}.$$

$\phi_0(\vec{\xi}, \alpha)$ is an even function and, due to Eq. (11), it obeys to

$$\int_{C_0} {\phi_0}^2(\vec{\xi}, \alpha) d^3\vec{\xi} = 1. \tag{30}$$

Substituting $(v_0/8)^{1/2} \phi_0(\vec{\xi}, \alpha)$ for $\phi(\mathbf{r}, \alpha)$ in Eq.s (20) and (27) and passing to new integration variable $\vec{\xi}$, one finds that

$$\epsilon_\sigma(r_s, \alpha) = \frac{e^2}{2a_0} \left[\frac{\tau_\sigma(\alpha)}{{r_s}^2} + \frac{v_\sigma(\alpha)}{r_s} \right] \tag{31}$$

where the dimensionless quantities $\tau_\sigma(\alpha)$ and $v_\sigma(\alpha)$ are

$$\tau_\sigma(\alpha) \equiv \kappa_\sigma \sum_{j,l=1}^{3} \int_{C_0} \mathcal{A}^\sigma_{j,l} (\partial_j \phi_0(\vec{\xi}, \alpha))(\partial_l \phi_0(\vec{\xi}, \alpha)) d^3\vec{\xi}, \tag{32}$$

$$\begin{aligned} v_\sigma(\alpha) \equiv \chi_\sigma \Bigg[{\sum_{\mathbf{m}}}' \int_{C_0} d^3\vec{\xi} \int_{C_0} d^3\vec{\xi}' \frac{{\phi_0}^2(\vec{\xi}, \alpha){\phi_0}^2(\vec{\xi}', \alpha) - {\phi_0}^2(\vec{\xi}, \alpha)/4 + 1/64}{d_\sigma(\vec{\xi} - \vec{\xi}' + 2\mathbf{m})} \\ - \int_{C_0} d^3\vec{\xi} \int_{C_0} d^3\vec{\xi}' \frac{{\phi_0}^2(\vec{\xi}, \alpha)/4 - 1/64}{d_\sigma(\vec{\xi} - \vec{\xi}')} \Bigg]. \end{aligned} \tag{33}$$

In these two equations, similarly to $M_{dl,\sigma}$'s definition, index σ ranges over $\{1,2,3\}$ respectively associated to lattices sc, bcc and fcc. Moreover, the partial derivatives present in Eq. (32) refer to variable $\vec{\xi}$ while the remaining symbols are defined as follows:

$$\kappa_1 = \Big(\frac{6}{\pi}\Big)^{2/3}, \quad {\mathcal{A}^{(1)}}_{j,l} = \delta_{j,l}, \quad \chi_1 = \Big(\frac{6}{\pi}\Big)^{1/3},$$
$$d_1(\vec{\xi}) \equiv \Big[\sum_{j=1}^{3} \xi_j^2\Big]^{1/2} \tag{34}$$

for the sc case,

$$\kappa_2 = \Big(\frac{3}{\pi}\Big)^{2/3}, \quad {\mathcal{A}^{(2)}}_{j,j} = 2, \text{ and } {\mathcal{A}^{(2)}}_{j,l} = 1 \text{ if } j \neq l, \quad \chi_2 = \Big(\frac{8}{\sqrt{3}\pi}\Big)^{1/3},$$
$$d_2(\vec{\xi}) \equiv \Big[\sum_{j=1}^{3} {\xi_j}^2 - \frac{2}{3} \sum_{1\leq j<l\leq 3} \xi_j \xi_l\Big]^{1/2} \tag{35}$$

for the bcc case, and

$$\kappa_3 = \Big(\frac{3}{2\pi}\Big)^{2/3}, \quad {\mathcal{A}^{(3)}}_{j,j} = 3 \text{ and } {\mathcal{A}^{(3)}}_{j,l} = -1 \text{ if } j \neq l, \quad \chi_3 = \Big(\frac{3\sqrt{2}}{\pi}\Big)^{1/3},$$
$$d_3(\vec{\xi}) \equiv \Big[\sum_{j=1}^{3} {\xi_j}^2 + \sum_{1\leq j<l\leq 3} \xi_j \xi_l\Big]^{1/2} \tag{36}$$

for the fcc case.
Numerically it is more convenient to express $\upsilon_\sigma(\alpha)$ in terms of Fourier transforms (FT) as we already showed in a first presentation[21] of the SLCQS approach based on quantum field theory but restricted to the only sc case. After denoting the FT of ${\phi_0}^2(\vec{\xi},\alpha)$ by $\widetilde{{\phi_0}^2}(\mathbf{q},\alpha)$, *i.e.*

$$\widetilde{{\phi_0}^2}(\mathbf{q},\alpha) = \int d^3\vec{\xi} e^{-i\mathbf{q}\cdot\vec{\xi}}\, {\phi^2}_0(\vec{\xi},\alpha), \tag{37}$$

in appendix A we show that $\upsilon_\sigma(\alpha)$ can be written as

$$\upsilon_\sigma(\alpha) = \upsilon_{P,\sigma}(\alpha) + \upsilon_{N,\sigma}(\alpha), \tag{38}$$

with

$$\upsilon_{P,\sigma}(\alpha) \equiv \chi'_\sigma {\sum_{\mathbf{m}}}' \frac{(\widetilde{{\phi_0}^2}(\pi\mathbf{m},\alpha))^2}{\tilde{d}^2{}_\sigma(\mathbf{m})}, \tag{39}$$

$$\upsilon_{N,\sigma}(\alpha) \equiv -\chi_\sigma \int_{C_0} d^3\vec{\xi} \int_{C_0} d^3\vec{\xi}' \frac{{\phi_0}^2(\vec{\xi},\alpha){\phi_0}^2(\vec{\xi}',\alpha)}{d_\sigma(\vec{\xi}-\vec{\xi}')}, \tag{40}$$

$$\tilde{d}^2{}_1(\mathbf{q}) \equiv {q_1}^2 + {q_2}^2 + {q_3}^2, \tag{41}$$

$$\tilde{d}^2{}_2(\mathbf{q}) \equiv \mathbf{q}\cdot\mathbf{q} + q_1q_2 + q_2q_3 + q_3q_1, \tag{42}$$

$$\tilde{d}^2{}_3(\mathbf{q}) \equiv \mathbf{q}\cdot\mathbf{q} - 2(q_1q_2 + q_2q_3 + q_3q_1)/3, \tag{43}$$

and

$$\chi_1{}' \equiv \chi_1/2\pi, \quad \chi_2{}' \equiv \sqrt{3}\chi_2/4\pi \quad \text{and} \quad \chi_3{}' \equiv 2^{2/3}\chi_3/6\pi. \tag{44}$$

After choosing a particular real even function $\phi_0(\vec{\xi},\alpha)$, which obeys Eq. (30) and vanishes with its first and second partial ξ-derivatives on the boundary of C_0, the best SLQC wave-function is obtained as follows. First, one evaluates quantities $\tau_\sigma(\alpha)$, $\upsilon_{P,\sigma}(\alpha)$ and $\upsilon_{N,\sigma}(\alpha)$ by Eq.s (32), (39) and (40) over a grid of α values: $\alpha_1,\ldots,\alpha_L$. Second, chosen an r_s value, by Eq.s (31), (32), (39) and (40) one obtains the set of values $\epsilon_\sigma(r_s,\alpha_i)$ with $i=1,\ldots,L$. The smallest of these values will correspond to a particular i denoted by $\bar{i}$. Then, $\epsilon_\sigma(r_s,\alpha_{\bar{i}})$ approximates the energy of the fundamental state for the considered SLQC wave-function with the considered crystalline symmetry, while $\alpha_{\bar{i}}$ represents the value of $\alpha_\sigma(r_s)$. Finally, the value of σ that yields the smallest energy at a fixed r_s value determines the crystalline symmetry of the jellium at the considered density.

3 Numerical results

We report now a numerical illustration of the procedure just described. To this aim we define function $\phi_0(\vec{\xi},\alpha)$ as follows

$$\phi_0(\vec{\xi},\alpha) \equiv \prod_{j=1}^{3} G(\xi_j,\alpha) \tag{45}$$

with

$$G(\xi,\alpha) \equiv C(\alpha)e^{-\alpha\xi^2/(1-\xi^2)}, \tag{46}$$

$$C(\alpha) \equiv \left(\sqrt{\pi}\Psi(1/2,0;2\alpha)\right)^{-1/2}, \tag{47}$$

where $\Psi(1/2,0;2\alpha)$ is a particular value of the confluent Hypergeometric function $\Psi(a,c;z)$ defined in §6.5 of Ref.[22]. The reported $C(\alpha)$ expression ensures that $\phi_0(\vec{\xi},\alpha)$ obeys condition (30). Besides, this function as well as all its partial derivatives vanish as $\vec{\xi}$ approaches the border of C_0. The factorized expression of $\phi_0(\vec{\xi},\alpha)$ further simplifies Eq.s (32), (37), (39) and (40). In fact, as shown in appendix B, $\tau_\sigma(\alpha)$ becomes

$$\tau_\sigma(\alpha) = \kappa'_\sigma\tau(\alpha) \equiv \kappa'_\sigma\left[2\int_0^1 [\partial_\xi G(\xi,\alpha)]^2 d\xi\right] \tag{48}$$

with $\kappa'_1 \equiv 3\kappa_1$, $\kappa'_2 \equiv 6\kappa_2$, $\kappa'_3 \equiv 9\kappa_3$ and

$$\tau(\alpha) = \frac{\Psi(-\frac{3}{2},\,-2;\,2\alpha)}{4\alpha\,\Psi(\frac{1}{2},\,0\,;\,2\alpha)}. \tag{49}$$

$\widetilde{\phi_0{}^2}(\mathbf{q},\alpha)$ becomes

$$\widetilde{\phi_0{}^2}(\mathbf{q},\alpha) = \prod_{j=1}^{3} \widetilde{G^2}(q_j,\alpha) \tag{50}$$

with

$$\widetilde{G^2}(q,\alpha) = \int_{-1}^{1} d\xi e^{-iq\xi} G^2(\xi,\alpha) = 2\int_0^1 d\xi \cos(q\xi) G^2(\xi,\alpha). \tag{51}$$

Besides, after putting for $0 \leq \eta \leq 2$

$$\Gamma(-\eta,\alpha) = \Gamma(\eta,\alpha) \equiv \int_{-1}^{1-\eta} G^2(\eta+\xi',\alpha) G^2(\xi',\alpha) d\xi', \tag{52}$$

Eq.s (39) and (40) respectively become

$$\upsilon_{P,\sigma}(\alpha) = \chi_\sigma {}' \sum_{\mathbf{m}}{}' \frac{\prod_{j=1}^{3} (\widetilde{G^2}(\pi m_j,\alpha))^2}{\tilde{d^2}_\sigma(\mathbf{m})}, \tag{53}$$

$$\upsilon_{N,\sigma}(\alpha) = -\chi_\sigma \int_{2C_0} d^3\vec{\eta} \frac{\prod_{l=a}^{3} \Gamma(\eta_l,\alpha)}{d_\sigma(\vec{\eta})}, \tag{54}$$

where $2C_0$ denotes the cubic cell $\{\vec{\eta}\,\big|\, -2 \leq \eta_i \leq 2,\ i=1,2,3\}$, and with the $\tilde{d^2}_\sigma(\mathbf{m})$s and $d_\sigma(\vec{\eta})$s defined by Eqs. (41)-(43) and (34)-(36).
In this way, we must numerically evaluate the 1D integral present on the rhs of (48) to determine $\tau_\sigma(\alpha)$, the 1D FT defined by Eq. (51) at a set of values $q = \pi m$ with $m = 0,\ldots,M$ to subsequently evaluate series (53) truncated at M, and, finally, $\Gamma(\eta,\alpha)$ at a set of points $\eta_1,\ldots,\eta_{M_I}$ lying within the interval [0,2] to evaluate 3D integral (54). (By so doing, we use the eveness of $\Gamma(\eta,\alpha)$ and $\widetilde{G^2}(q,\alpha)$ with respect to η and q.) The calculations must performed over a grid of α values: $0 < \alpha_1 < \ldots < \alpha_L$. After numerically determining $\tau_\sigma(\alpha_i)$ by Eq. (48), $\upsilon_{P,\sigma}(\alpha_i)$ by Eq. (53) and $\upsilon_{N,\sigma}(\alpha_i)$ by Eq. (54), we look for the minimum value of

$$\epsilon_\sigma(r_s,\alpha_i) = \frac{\tau_\sigma(\alpha_i)}{{r_s}^2} + \frac{\upsilon_{P,\sigma}(\alpha_i) + \upsilon_{N,\sigma}(\alpha_i)}{r_s} \tag{55}$$

at a fixed r_s value as i ranges from 1 to L. Then, as already reported at the end of the previous section, if the minimum occurs at $i = \bar{i}$, the SLQC fundamental state corresponds to Eq. (6) with $\alpha = \alpha_{\bar{i}}$ and the corresponding energy per particle, in Rydberg units, is $\epsilon_\sigma(r_s,\alpha_{\bar{i}})$. Changing the r_s value, $\bar{i}$ will also change and the set of the $\alpha_{\bar{i}}$ values numerically determines $\alpha_\sigma(r_s)$, *i.e.* the way α_σ changes with r_s is determined by the set of values $\alpha_{\bar{i}}$ relevant to the considered lattice symmetry.
Before illustrating our numerical results, we give some details about numerical computations. We considered an α grid that spans the interval [0.01, 500] at integer multiples of 0.05 up to $\alpha = 0.5$, of 0.1 up to $\alpha = 2$, of 1 up to $\alpha = 20$, of 10 up to $\alpha = 100$ and of 100 up to $\alpha = 500$. The numerical accuracy of the results, depending on the values of M, M_I and the number of points used to evaluate quantities $\tau(\alpha)$, $\widetilde{G^2}(q,\alpha)$, $\Gamma(\eta,\alpha)$ and $\upsilon_\sigma(\alpha)$, was tested at $\alpha = 0.01$ and 100. The first six significant digits of $\tau(\alpha)$ do not change passing from 10^8 to 10^9 points. The first 5 digits of the FTs evaluated with 10^6 or 10^7 points do

not differ and agree with their asymptotic formula given by Eq. (96) of [21] [note that here the correct argument of the sine function is $(2 + \sqrt{2q\alpha} - \pi/8)$]. The first five digits of the resulting $\upsilon_{P,\sigma}(\alpha)$ values, obtained truncating the series at $M = 50$ or $M = 100$, also coincide. The calculation of $\upsilon_{N,\sigma}(\alpha)$ requires more care. The evaluation of $\Gamma(\eta)$ with integration steps of 10^{-5} or 10^{-6} leaves the first five digits unchanged. However, the evaluation of the remaining 3D integral over $\vec{\eta}$ cannot be done with an integration step $\Delta\eta$ smaller than 10^{-4} because the required CPU time becomes very large. Thus we made three runs with $\Delta\eta$ respectively equal to 1/500, 1/1000 and 1/1500. The first four digits do not change even at large αs, *i.e.* $\alpha \geq 100$, which is the critical region. The ratio of the resulting errors, defined as (second -fist)run divided by (third - first)run, was found fairly equal to 3/2. In this way we numerically extrapolated the results to $\Delta\eta \to 0$. The resulting $\upsilon_{N,\sigma}(\alpha)$ values ought to have five correct digits. $\upsilon_{P,\sigma}(\alpha)$ and $\upsilon_{N,\sigma}(\alpha)$ always have opposite signs. At large αs, they have the first two digits equal. Hence, the final $\upsilon_{\sigma}(\alpha)$ values have the first three digits exact for all the considered values of α.

We pass now to illustrate our results. These are shown in Fig.s 1a, 1b and 2. Fig.s 1a and 1b respectively show the energy per particle (in Rydberg units) *versus* r_s, in the high density region, and *vs* $Lg_{10}(r_s)$ in the low density one. In fact, the continuous and dotted curves refer to Bloch's expression (3) and Carr's expression (5), respectively. The long-dash curves refer to the optimized SLQC wave-function with symmetry bcc, and the short-dash curves to the simple cubic optimized SLQC wave-function. The full triangles and circles are the values respectively obtained for the fluid and bcc crystalline phases by QMC calculations[11, 12, 15, 16]. (We have not reported the curve relevant to the fcc SLQCS solution in order to not overcrowd the figure. It lies close to the bcc solution.) The short-dash curve crosses the continuous one at $r_s = 28$ and for greater r_s values it lies below the continuous curve. On the basis of the Ritz-Rayleigh principle one concludes that the SLQCS with the sc symmetry is closer to the true fundamental state than $|F_p\rangle$. In other words, as the density decreases, the jellium passes from the polarized fluid phase to the sc crystalline one at $r_s = 28$. The figures also show that long-dash curve passes from above to below the continuum one at $r_s = 38$. This means that in the region $28 < r_s < 38$, the sc phase is more stable than the fluid which in turn is more stable than the bcc. In the region $r_s > 38$, the bcc phase is more stable than the fluid and is less stable than the sc up to $r_s = 500$. The figures make also evident a property that appears to have been overlooked by most textbooks: Carr's approximation appears to be surprisingly accurate throughout the full density range since it fairly agrees with QMC results even at high densities.

We pass now to the illustration of figure 2. The full triangles and the close dotted line respectively represent $\alpha_2(r_s)$ and $\alpha_1(r_s)$ on a log-log scale. The apparent step behaviour is an artifact of the chosen α-grid whose values are not equally spaced. One should note, at large $Lg_{10}(r_s)$s, the approximate linear behaviour of $Lg_{10}(\alpha)$ with a slope corresponding to have $\alpha_\sigma \propto {r_s}^{1/2}$. The continuous and the long-dash curve reported on the top of the figure respectively plot $\upsilon_2(\alpha)$ and $\upsilon_1(\alpha)$ *vs.* $Lg_{10}(\alpha)$. These curves can also be considered as the plots of $\upsilon_\sigma(\alpha(r_s))$

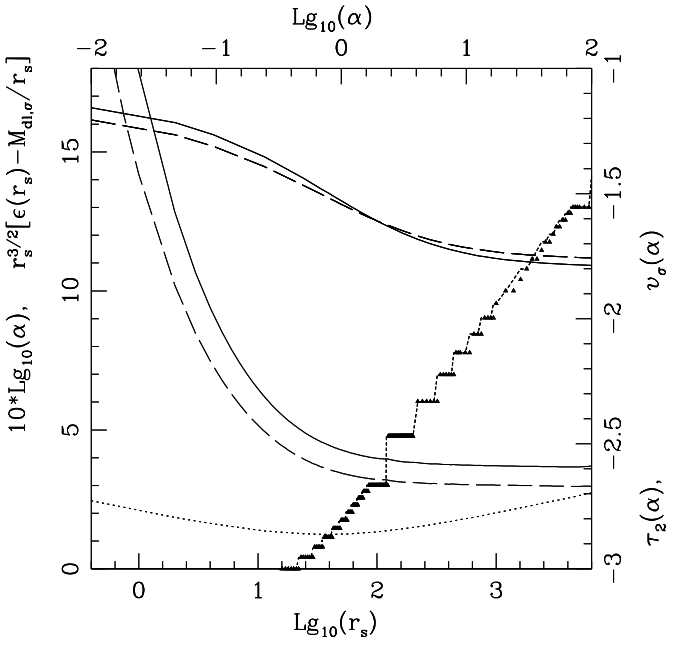

Figure 2: The dotted step-line and the full triangles are the plots of $10 \times Lg_{10}(\alpha_\sigma)$ *vs.* $Lg_{10}(r_s)$ for the sc and bcc case; the continuous and the long-dash curves (convex and monotonically decreasing) those of $r_s^{3/2}[\epsilon_\sigma(r_s)+M_{dl,\sigma}/r_s]$ *vs.* $Lg_{10}(r_s)$ for the bcc ($\sigma = 2$) and sc case ($\sigma = 1$) [the corresponding vertical scale is on the left and the energy units are ryd]; the continuum and the long-dash sigmoidal curves those of $\upsilon_2(\alpha)$ and $\upsilon_1(\alpha)$ *vs.* $Lg_{10}(\alpha)$ (the relevant horizontal and vertical scales are the top and the right ones); finally, the parabolic dotted curve that of $Lg_{10}(\tau_2(\alpha))$ *vs.* $Lg_{10}(\alpha)$ (its vertical scale is the left one).

vs. r_s for the noted property that $\alpha_\sigma \propto {r_s}^{1/2}$. In this way, the figure makes it evident that the SLQCS $\upsilon_\sigma(r_s)$s approach the relevant Madelung values as $r_s \to \infty$. The remaining two monotonically decreasing convex curves are the plots of $r_s^{3/2}[\epsilon_\sigma(r_s) + M_{dl,\sigma}/r_s]$ em vs. r_s for the bcc (continuous curve) and the sc (dotted) symmetry. The constant behaviour observed at large r_s values indicates that

$$\epsilon_\sigma(r_s) \approx -\frac{M_{dl,\sigma}}{r_s} + \frac{\mathcal{C}_\sigma}{{r_s}^{3/2}} + o\big(\frac{1}{{r_s}^{3/2}}\big), \tag{56}$$

the $\mathcal{C}_\sigma$s being appropriate constants that from the figure appear to be equal to 3.6 and 2.9 for $\sigma = 2$ and 1, respectively. In appendix B we show that the SLQCS procedure always yields an energy per particle that asymptotically behaves as reported in Eq. (56) at large r_s. It is stressed that this behaviour coincides with that of Eq.s (4) and (5), even though the numerical coefficients of the $r_s^{-3/2}$ contribution are different. In this respect, we recall that the crystalline HF solutions investigated in Ref.[10] also behave as in Eq. (56) and from Fig.4 of this paper it appears that $\mathcal{C}_2 \approx 3$. We once more underline that contribution $-M_{dl,2}/r_s$ comes naturally out by the HF and the SLQCS procedure [that is equivalent to a Hartree or a HF equation as explained below Eq. (23)], while in Wigner's and Carr's derivation of Eq.s (4) and (5) it was put there because it is the energy of the 'static' unperturbed Hamiltonian.
Finally, the dotted parabolic curve plots $Lg_{10}(\tau_2(\alpha))$ *vs* $Lg_{10}(\alpha)$. It shows a linear behaviour in the outermost α range that follows from Eq. (49) as we explicitly show in appendix B.

4 Conclusion

As Wigner first pointed out, an overall neutral one component plasma of electrons shows, at $T = 0^0 K$, the interesting feature of being in a crystalline phase as the particle number density becomes smaller than a particular value. This feature can nowadays be considered well assessed because it was confirmed by HF and QMC calculations (though the transition density is not accurately known yet). The fact that quantum Coulombic crystals exist at very high dilution, on physical grounds, has the important consequence that their behaviours must approach those of the corresponding classic Coulombic crystals. In fact, in the infinite dilution limit, the inter-electron mean distance becomes infinitely large with the consequence that: the overlapping among the the wave-functions of different electrons is expected to vanish and electrons become distinguishable in the sense that one can speak of an electron that occupies a well definite region/cell of the crystal. The SLQCS approach exactly captures the last two features. In fact, the SLQCS is completely antisymmetric but the support properties of the involved wave-functions make the fully antisymmetric wave-function equivalent to the Hartree one. Consequently, the electrons behave as particles each of them being confined to a single cell of the crystal. The determination of the *best* SLQCS, equivalent to solve the corresponding Hartree or Hartree-Fock equation, proceeds by a simple variational procedure. In fact, we worked out

the expression, in an integro-differential form, of the energy per particle, given by Eq. (31) together with Eq.s (32)-(43), in terms of the basic function $\phi(\mathbf{r},\alpha)$ different from zero only within a single primitive cell and depending on a real parameter α. The solution was obtained by looking for the minimum of the energy with respect to α at each fixed r_s value. The results illustrated in the three figures show that, at large r_ss, the leading term of the SLQCS energy per particle coincides with that of Eq.s(4) and (5) with an important difference: Wigner and Carr took this contribution from the classical Coulombic crystal's value while the SLQCS procedure directly produces this term. Moreover, as shown in appendix B, this procedure also implies that the next to the leading asymptotic term of $\epsilon_\sigma(r_s)$ behaves as $C_\sigma/{r_s}^{3/2}$. The r_s dependence coincides with that of Wigner's and Carr's formulae but the numerical values of coefficient C_σ are different. These values are also different from the values obtained solving the HF equation[10]. Hence, in the very low density region, the differences among the Wigner/Carr, the SLQCS and the HF approximations of the jellium model set only into at the level of the $O({r_s}^{-3/2})$ term. We consider this result as the main conclusion of this analysis. The implications of this conclusion are: Wigner or Carr formulae are equally accurate in the far r_s region though the dominating contribution was not quantum-mechanically derived; the SLQCS approach quantum-mechanically derives this contribution and therefore it is there as accurate as the HF equation but of simpler application; as the system becomes denser the numerical differences in coefficient C_σ make the approximations no longer equivalent. One expects that overlapping effects be no longer negligible and that the SLQCS approach drastically deteriorates in comparison to the HF one.

A Conversion of Eq. (33) in Eq.s (39) and (40)

To write Eq.s (33) in a form more convenient for numerical computations, we first introduce function $\Theta_0(\vec{\xi})$, equal to 1 if $\vec{\xi}$ lies within C_0 and equal to zero elsewhere. After putting

$$\Psi(\vec{\xi},\alpha) \equiv {\phi_0}^2(\vec{\xi},\alpha) - \Theta_0(\vec{\xi})/8, \tag{57}$$

one easily proves that the quantity inside the square brackets on the rhs of Eq. (33) can be written as

$$\sum_{\mathbf{m}} \int_{C_0} d^3\vec{\xi} \int_{C_0} d^3\vec{\xi}' \frac{\Psi(\vec{\xi},\alpha)\Psi(\vec{\xi}',\alpha)}{d_\sigma(\vec{\xi}-\vec{\xi}'+2\mathbf{m})} - \int_{C_0} d^3\vec{\xi} \int_{C_0} d^3\vec{\xi}' \frac{{\phi_0}^2(\vec{\xi},\alpha){\phi_0}^2(\vec{\xi}',\alpha)}{d_\sigma(\vec{\xi}-\vec{\xi}')}, \tag{58}$$

where the sum includes now the term with $\mathbf{m}=\mathbf{0}$. Since $\phi_0(\vec{\xi},\alpha)$ and $\Theta_0(\vec{\xi})$ are equal to zero outside C_0, integrals in Eq. (58) can be extended to the full R^3. The FT transform of $\Psi(\vec{\xi},\alpha)$ will be denoted by $\tilde{\Psi}(\mathbf{q},\alpha)$. Both $\phi_0(\vec{\xi},\alpha)$ and $\Theta_0(\vec{\xi})$ are real and even function of $\vec{\xi}$. Then $\tilde{\Psi}(\mathbf{q},\alpha)$ is an even function of $\mathbf{q}$.

Using the FTs, the generic term of the series can be written as

$$\frac{1}{(2\pi)^6}\int_{R^3} d^3\vec{\xi}\int_{R^3} d^3\vec{\xi}'\frac{1}{d_\sigma(\vec{\xi}-\vec{\xi}'+2\mathbf{m})}\int d^3\mathbf{q}e^{i\mathbf{q}\cdot\vec{\xi}}\,\tilde{\Psi}(\mathbf{q},\alpha)\int d^3\mathbf{q}'e^{-i\mathbf{q}'\cdot\vec{\xi}'}\,\tilde{\Psi}(\mathbf{q}',\alpha). \tag{59}$$

The change of the integration variable $\vec{\xi}\rightarrow\vec{\eta}=\vec{\xi}-\vec{\xi}'+2\mathbf{m}$ allows us to perform the $\vec{\xi}'$ integration so as to convert the previous expression into

$$\frac{1}{(2\pi)^3}\int_{R^3} d^3\vec{\eta}\int d^3\mathbf{q}\frac{1}{d_\sigma(\vec{\eta})}e^{i\mathbf{q}\cdot(\vec{\eta}-2\mathbf{m})}\,\tilde{\Psi}^2(\mathbf{q},\alpha).$$

The integral over $\vec{\eta}$ yields

$$\frac{1}{(2\pi)^3}\int_{R^3} d^3\vec{\eta}\frac{1}{d_\sigma(\vec{\eta})}e^{i\mathbf{q}\cdot\vec{\eta}}=\frac{4\pi}{(2\pi)^3}\frac{\omega_\sigma}{\tilde{d^2}_\sigma(\mathbf{q})}$$

with

$$\omega_1\equiv 1,\quad \omega_2\equiv\sqrt{3}/2,\quad \omega_3\equiv 2^{2/3}/3, \tag{60}$$

and the $\tilde{d^2}_\sigma(\mathbf{q})$s defined by Eq.s (41)-(43). In this way, the series present in Eq. (58) converts in

$$\frac{4\pi\omega_\sigma}{(2\pi)^3}\int d^3\mathbf{q}\frac{\tilde{\Psi}^2(\mathbf{q},\alpha)}{\tilde{d^2}_\sigma(\mathbf{q})}\sum_{\mathbf{m}}e^{-i2\mathbf{m}\cdot\mathbf{q}}. \tag{61}$$

Using the mathematical identity[5]

$$\sum_{\mathbf{m}}e^{i2\mathbf{m}\cdot\mathbf{q}}=\frac{(2\pi)^3}{8}\sum_{\mathbf{m}}\delta(\mathbf{q}-\pi\mathbf{m}) \tag{62}$$

the integrals over $\mathbf{q}$ in Eq. (61) are immediately evaluated if $\mathbf{m}\neq\mathbf{0}$, while the contribution relevant to $\mathbf{m}=\mathbf{0}$ is equal to zero because the resulting integrand $\tilde{\Psi}^2(\mathbf{q},\alpha)/\tilde{d^2}_\sigma(\mathbf{q})$ vanishes at $\mathbf{q}=\mathbf{0}$. In fact, condition (30) and the definition of $\Theta_0(\vec{\xi})$ imply that

$$\tilde{\Psi}(\mathbf{0},\alpha)=\int_{C_0} d^3\vec{\xi}\,\left[{\phi_0}^2(\vec{\xi},\alpha)-\Theta_0(\vec{\xi})/8\right]=0.$$

Moreover the eveness and the reality of $\phi_0(\vec{\xi},\alpha)$ and $\Theta_0(\vec{\xi})$ ensure that

$$\tilde{\Psi}(\mathbf{q},\alpha)=\widetilde{{\phi_0}^2}(\mathbf{q},\alpha)-\widetilde{\Theta_0}(\mathbf{q})/8\approx O(\mathbf{q}\cdot\mathbf{q})$$

at small $|\mathbf{q}|$. This property implies that

$$\frac{\tilde{\Psi}^2(\mathbf{q},\alpha)}{\tilde{d^2}_\sigma(\mathbf{q})}\approx O(|\mathbf{q}|^2)$$

and one concludes that no contribution to the sum over $\mathbf{m}$ arises from the term with $\mathbf{m} = \mathbf{0}$. Thus, the series present in Eq. (58) is equal to

$$\frac{\omega_\sigma}{2\pi} {\sum_{\mathbf{m}}}' \frac{\tilde{\Psi}^2(\pi\mathbf{m}, \alpha)}{\tilde{d^2}_\sigma(\mathbf{m})}. \tag{63}$$

A further simplification follows from the analytic expression of $\widetilde{\Theta_0}(\mathbf{q})$. This reads

$$\widetilde{\Theta_0}(\mathbf{q}) = \prod_{j=1}^{3} \int_{-1}^{1} e^{-iq_j\xi} d\xi = 8 \prod_{j=1}^{3} \frac{\sin(q_j)}{q_j}.$$

Since $\widetilde{\Theta_0}(\pi\mathbf{m}) = 0$ if $\mathbf{m} \neq \mathbf{0}$, we can replace $\tilde{\Psi}^2(\pi\mathbf{m}, \alpha)$ with $(\widetilde{{\phi_0}^2}(\pi\mathbf{m}, \alpha))^2$ in Eq. (64) and finally write Eq. (58) as

$$\left[\frac{\omega_\sigma}{2\pi} {\sum_{\mathbf{m}}}' \frac{(\widetilde{{\phi_0}^2}(\pi\mathbf{m}, \alpha))^2}{\tilde{d^2}_\sigma(\mathbf{m})}\right] - \int_{C_0} d^3\vec{\xi} \int_{C_0} d^3\vec{\xi}' \frac{{\phi_0}^2(\vec{\xi}, \alpha){\phi_0}^2(\vec{\xi}', \alpha)}{d_\sigma(\vec{\xi} - \vec{\xi}')}. \tag{64}$$

Expression (38) for $\upsilon_\sigma(\alpha)$ and Eq.s (39) and (40) for $\upsilon_{P,\sigma}(\alpha)$ and $\upsilon_{N,\sigma}(\alpha)$ immediately follow from Eq. (64) recalling that Eq. (58) is the content of the square brackets in Eq. (33).

B Asymptotic behaviour of $\epsilon_\sigma(r_s)$ at large r_s

First of all Eq.s (47) and (49) are derived as follows. The condition that $\phi_0(\xi, \alpha)$ be normalized requires that $G(\xi, \alpha)$ be normalized and this implies that

$$C^{-2}(\alpha) = 2 \int_0^1 e^{-2\alpha x^2/(1-x^2)} dx. \tag{65}$$

With the change of the integration variable: $x \to \sqrt{y}/\sqrt{1+y}$, the above expression converts to

$$C^{-2}(\alpha) = \int_0^\infty y^{-1/2}(1+y)^{-3/2} e^{-2\alpha y} dy. \tag{66}$$

Recalling the general definition of the confluent hypergeometric function $\Psi(a, b; z)$

$$\Psi(a, b; z) \equiv \frac{1}{\Gamma(a)} \int_0^\infty e^{-xt} t^{a-1} (1+t)^{c-a-1} dt, \tag{67}$$

reported in §6.5 of Ref.[22], from Eq. (66) immediately follows that

$$C^{-2}(\alpha) = \sqrt{\pi}\Psi(\frac{1}{2}, 0; 2\alpha), \tag{68}$$

which is equivalent to Eq. (47). In the same way,

$$2 \int_0^1 \left[\partial_x G(x, \alpha)\right]^2 dx = 2C^2(\alpha) \int_0^1 \left[\frac{2\alpha x e^{-\alpha x^2/(1-x^2)}}{1-x^2}\right]^2 dx \tag{69}$$

and, by the previous change of the integration variable, one finds

$$2C^2(\alpha)\int_0^1 \left[2\alpha^2 e^{-2\alpha y} y^{1/2}(1+y)^{3/2}\right]^2 dy$$
$$= C^2(\alpha)\sqrt{\pi}\Psi(-\frac{3}{2},\,-2\,,\,2\alpha) = \frac{\Psi(-\frac{3}{2},\,-2\,,\,-2\alpha)}{4\alpha\Psi(\frac{1}{2},\,0\,,\,2\alpha)}, \qquad (70)$$

i.e. Eq. (49).
Finally we show that the SLQCS approximation implies that $\epsilon_\sigma(r_s)$ at large r_s behaves according to Eq. (56). Once we have determined $\alpha_\sigma(r_s)$, from Eq. (31) follows that

$$\epsilon_\sigma(r_s) = \frac{e^2}{2a_0}\left[\frac{\tau_\sigma(\alpha(r_s))}{{r_s}^2} + \frac{\upsilon_\sigma(\alpha(r_s))}{r_s}\right], \qquad (71)$$

while the $\alpha_\sigma(r_s)$s are determined solving the equations

$$\frac{\partial}{\partial\alpha}\left(\frac{\tau_\sigma(\alpha)}{r_s^2} + \frac{\upsilon_\sigma(\alpha)}{r_s}\right) = 0. \qquad (72)$$

Illustrating Fig. 2's results, we already noted that $\lim_{\alpha\to\infty}\upsilon_\sigma(\alpha) = -M_{dl,\sigma}$ and that $\alpha \approx {r_s}^{1/2}$ at large r_s. Besides, based on the fact that the $\upsilon_\sigma(r_s)$s approach their limit values from the above, after putting $\beta \equiv 1/\alpha$ it appears reasonable to assume for the $\upsilon_\sigma(\alpha)$s, as $\beta \to 0^+$, the following asymptotic behaviour

$$\upsilon_\sigma(\alpha) \approx -M_{dl,\sigma} + c_\sigma\beta + o(\beta), \qquad (73)$$

c_σ being a positive constant. The asymptotic behaviour of $\tau_\sigma(\alpha)$ at large α is easily obtained from that of $\Psi(a,,b;\,2\alpha)$, reported in §6.13.1 of Ref.[22]. One finds that

$$\tau_\sigma(\alpha) \approx \kappa_\sigma\left[\frac{1}{\beta} + \frac{3}{2} + \frac{9\beta}{16} + o(\beta)\right]. \qquad (74)$$

Eq.s (73) and (74) allow us to evaluate the derivatives present in Eq. (72) so that this equation, to the leading order, converts into $-\kappa_\sigma/(\beta^2 r_s^2) + c_\sigma/r_s = 0$. The solution is

$$\alpha = \sqrt{c_\sigma r_s/\kappa_\sigma}. \qquad (75)$$

Its substitution in Eq. (71) yields the first two leading terms of the asymptotic expansion of $\epsilon_\sigma(r_s)$ at large r_s, ie

$$\epsilon_\sigma(r_s) \approx \frac{e^2}{2a_0}\left[-\frac{M_{dl,\sigma}}{r_s} + \frac{\sqrt{\kappa_\sigma c_\sigma}}{r_s^{3/2}} + \cdots\right]. \qquad (76)$$

This result shows that the SLQCS approach implies that, at very high dilution, the leading term of the energy per particle is the classical Madelung value and that the leading correction to this term decreases as ${r_s}^{-3/2}$ with a positive numerical factor equal to $\sqrt{\kappa_\sigma c_\sigma}$. Fig.2 results indicate that this factor nearly equals 2.9 and 3.6 in the sc and bcc case, respectively.

References

[1] A.L. Fetter and J.D. Walecka, *Quantum Theory of Many-Particle Systems*, McGraw-Hill, New York, (1971).

[2] G.D. Mahan, *Many-particle Physics*, Plenum Press, New York, (1981).

[3] E.P. Wigner, *Phys. Rev.*, **46**, 1002, (1934).

[4] F. Bloch, *Z. Physik* **57**, 545, (1929).

[5] M.P. Marder, *Condensed Matter Physiscs*, Wiley, New York, (2000).

[6] E.P. Wigner, *Trans. Farad. Soc.* **34**, 678, (1938).

[7] W.J. Carr, *Phys. Rev.* **122**, 1437, (1961).

[8] A. Messiah, *Mécanique Quantique*, vol. II, Dunod, Paris, (1962).

[9] W.M.C. Foulkes, L. Mitas, R.J. Needs and G. Rajagopal, *Rev. Mod. Phys.* **73**, 33,(2001).

[10] J.R. Trail, M.D. Towler and R.J. Needs, *Phys. Rev. B* **68**, 045107, (2003).

[11] D.M. Ceperley and B.J. Alder, *Phys. Rev. Lett.* **45**, 567, (1980).

[12] G. Ortiz and P. Ballone, *Phys. Rev. B* **50**, 1391, (1994).

[13] Y. Kwon, D.M. Ceperley and R.M. Martin, *Phys. Rev B* **58**, 6800, (1998).

[14] G. Ortiz, M. Harris and P. Ballone, *Phys. Rev. Lett.* **82**, 5317, (1999).

[15] F.H. Zong, C. Lin and D.M. Ceperley, *Phys. Rev. E* **66**, 036703, (2002).

[16] N.D. Drummond, Z. Radnai, J.R. Trail, M.D. Towler and R.J. Needs, *Phys. Rev. B* **69**, 085116, (2004).

[17] C. Kittel, *Introduction to Solid State Physics*, J. Wiley, New York, (2005).

[18] J. Kohanoff, *Electronic Structure Calculations for Solid and Molecules*, Cambridge Univ. Press, Cambridge, (2006), §3.1.

[19] J.C. Slater, *Insulators, Semiconductors and Metals. Quantum Theory of Molecules and Solids*, (McGraw Hill, New York, 1967).

[20] N.W. Ashcroft, and N.D. Mermin, *Solid State Physics*, Harcourt Coll. Pub., New York, 1976.

[21] S. Ciccariello, arXiv:0712.1463v1 [cond-matt.str-el] (2007).

[22] A. Erdéley, W. Magnus, F. Oberhettinger, F.G. Tricomi, *Higher Transcendental Functions I*, McGraw-Hill, New York, (1953).